View metadata, citation and similar papers at core.ac.uk
brought to you by CORE
provided by Texas A&M Repository

PHYSICAL REVIEW C **80**, 024306 (2009)

Continuum spectroscopy with a ^{10}C beam: Cluster structure and three-body decay

R. J. Charity, T. D. Wiser, K. Mercurio, R. Shane, and L. G. Sobotka
Departments of Chemistry and Physics, Washington University, St. Louis, Missouri 63130, USA

A. H. Wuosmaa
Department of Physics, Western Michigan Uinveristy, Kalamazoo, Michigan 49008, USA

A. Banu, L. Trache, and R. E. Tribble
Cyclotron Institute, Texas A&M University, College Station, Texas 77843, USA
(Received 24 April 2009; published 14 August 2009)

Resonance-decay spectroscopy is used to study particle-unbound excited states produced in interactions of $E/A = 10.7$ MeV ^{10}C on Be and C targets. After inelastic scattering, structures associated with excited states in ^{10}C were observed at 5.22, 5.29, 6.55, 6.56, 6.57, and 8.4 MeV which decay into the $2p + 2\alpha$ final state. This final state is created via a number of different decay paths, which include prompt and sequential two-proton decay to the ground state of ^{8}Be, α decay to ^{6}Be$_{\text{g.s.}}$, and proton decay to the 2.345-MeV state of ^{9}B. For the sequential two-proton decay states (5.22 and 6.55 MeV), angular correlations between the first two decay axes indicate that the spin of these states are nonzero. For the prompt two-proton decay of the 5.29-MeV state, the three-body correlations between the two protons and the core are intermediate between those measured for ground-state ^{6}Be and ^{45}Fe decays. The 6.55- and 6.57-MeV structures are most probably associated with the same level, which has a 14% two-proton decay branch with a strong "diproton" character and a 86% sequential two-proton decay branch. Correlations between the fragments following the three-body decay of the 2.345-MeV state of ^{9}B can be approximately described by sequential α decay to the ^{5}Li intermediate state. The 8.06- and 9.61-MeV ^{10}B states that decay into the $d + {}^{6}\text{Li}_{2.186}$ channel are confirmed. Evidence for cluster structure in ^{13}N is obtained from a number of excited states that decay into the $p + 3\alpha$ exit channel.

DOI: 10.1103/PhysRevC.80.024306 PACS number(s): 21.10.−k, 25.70.Ef, 25.60.−t, 27.20.+n

I. INTRODUCTION

For experiments performed with poor quality secondary beams, resonance-decay spectroscopy provides a method for studying the levels of exotic nuclei that particle decay [1–4]. This method involves the detection of all the decay products, and the excitation energy is determined from their invariant mass. The excitation-energy resolution is dependent on the decay channel and the angle and velocity of the decaying fragment, but otherwise it is independent of how the fragment was created. The resolution is limited by the target thickness and the angular and energy resolving powers of the detector array and is often estimated from Monte Carlo simulations.

In this work we will discuss results obtained with resonance-decay spectroscopy using a ^{10}C beam. Particular attention will be focused on ^{10}C excited states for which the level scheme is poorly known. Above 3.726 MeV, the excited states of ^{10}C are particle unbound. Below 15 MeV, where the ^{3}He + ^{7}Be decay channel opens, all particle-unbound levels eventually decay into the $2p + 2\alpha$ final state, as all possible intermediate states are also particle unstable.

Apart from ^{10}C levels, many other states in other nearby nuclei were observed. Of these, we will report on data for the ^{10}B and ^{13}N states for which new information was obtained.

Excited states with cluster structures are of particular interest. Such states often appear as narrow levels just above the cluster breakup threshold [5]. For two, three, or more α clusters, many configurations have been predicted with the excess neutrons occupying molecular-like orbits [6]. While theoretical studies have focused more on the neutron-rich isotopes, in practice experimental resonance-decay spectroscopy is easier for the proton-rich mirror states, as protons are easy to detect with excellent energy and angular resolution. Cluster structure has been studied both experimentally and theoretically in the mirror nuclei ^{10}Be and ^{13}C of ^{10}C and ^{13}N [6], respectively.

Previously we reported evidence for prompt two-proton decay of ^{10}C excited states [7]. Prompt decay occurs when the two protons are emitted simultaneously. This must be differentiated from sequential decay, which refers to a time-ordered process where after the emission of the first proton there exists a long-lived ^{9}B intermediate state. For example, assuming this intermediate is the ground state ($\Gamma = 0.5$ keV), then it will not decay until the proton emitted in the initial step is of the order of 10^{4} fm away. Thus for two-proton decay, the $^{9}\text{B}_{\text{g.s.}}$ lifetime of 1.2×10^{-18} s is considered long, and the two proton-emission steps will be uncorrelated apart from constraints due to conservation laws. For a sequential decay through a ^{9}B excited state of $\Gamma \sim 1$ MeV (lifetime $\sim 10^{-21}$ s), the first proton travels only on the order of the ^{10}C diameter before the second proton is emitted. In this case, time ordering becomes unclear, and the presence of the first proton can influence the subsequent proton decay of ^{9}B. Thus the concept of sequential decay breaks down if the lifetime of the intermediate state is too short; there is not a sharp boundary between sequential and prompt decay processes, and one merges with the other as the time scales change.

 ©2009 The American Physical Society

In this work, we have repeated our original ^{10}C experiment and obtained a significantly larger number of events for prompt two-proton decay thus confirming our original results. The three-body decay of ^{6}Be$_{g.s.}$ and the 2.345-MeV state of ^{9}B were also observed in this experiment. The results for ^{6}Be$_{g.s.}$ and a comparison with the predictions of a three-body cluster model have been presented elsewhere [8,9]. The results for ^{9}B are presented in this work.

The experimental method is briefly described in Sec. II, and results for ^{10}C, ^{10}B, and ^{13}N are presented in Sec. III. Finally, the conclusions are listed in Sec. IV. Some aspects of this work have been published in rapid form [10].

II. EXPERIMENTAL METHOD

The Texas A&M University K500 cyclotron facility was used to produce a 200-pnA beam of ^{10}B at $E/A = 15.0$ MeV. This primary beam impinged on a hydrogen gas cell held at a pressure of 2 atm and kept at liquid-nitrogen temperature. A secondary beam of $E/A = 10.7$ MeV ^{10}C was produced through the ^{10}B$(p, n)^{10}$C reaction and separated from other reaction products using the momentum achromat recoil spectrometer (MARS) [11]. This secondary beam, with intensity of 2×10^5 s^{-1}, purity of 99.5%, an energy spread of 3%, and a spot size of 3.5×3.5 mm, interacted with either a 14.1-mg/cm^2 Be or a 13.4-mg/cm^2 C target.

The reaction products were detected in an array of four Si E-ΔE telescopes located in a plane 14 cm downstream of the target. The telescopes, part of the High Resolution Array (HiRA) [12], consisted of a 65-μm-thick, single-sided Si-strip ΔE detector followed by a 1.5-mm-thick, double-sided Si strip E detector. All Si detectors were 6.4×6.4 cm in area with their position-sensitive faces divided into 32 strips. The telescopes were positioned in a square arrangement, with each telescope offset from its neighbor to produce a small, central, square hole through which the unscattered beam passed. This detector arrangement covered from $\theta = 1.3^\circ$ to 7.7°. More details of the experimental arrangement can be found in Ref. [10].

The number of ^{10}C particles incident on the Be and C targets was determined indirectly by measuring the intensity of the primary ^{10}B beam in a Faraday cup after the gas cell and normalizing the yield, at low beam intensity, by directly counting the ^{10}C particles with a detector located in the target position.

III. RESULTS

Evidence for particle-unbound excited states can be found from the correlations between the decay products. The excitation energy is reconstructed from the kinetic energies of these fragments in their center-of-mass frame after the decay Q value is subtracted. We present in the following, excitation-energy distributions obtained from pairs, triplets, and quadruplets of particles detected in coincidence. Peaks observed in these distributions will be compared with the compiled levels in Refs. [13,14]. In some cases, new levels are observed. Table I lists the properties of states for which new information is determined. Excitation-energy spectra presented in this work are associated with the combined data from both the Be and C targets unless otherwise specified.

Monte Carlo simulations were performed to estimate the experimental excitation-energy resolution and the detection efficiency. These include the effect of the beam-spot size, energy loss [15], and small-angle scattering in the target [16], and the angular and energy resolution of the detector array. These simulations are discussed in more detail in Ref. [7], where they are shown to be accurate for a number of known narrow levels. These results are used to extract the experimental widths and cross sections for the new levels reported in this work. The predicted excitation-energy

TABLE I. Excitation energy, width, cross sections for Be and C targets, and spin of states for which new information is determined.

Nucleus	$\langle E^* \rangle$[a] (MeV)	Γ (keV)	Initial decay	Exit channel	σ_{Be} (μb)	σ_C (μb)	J
^{10}B	8.06 ± 0.05	379 ± 50	$d + {}^{6}\mathrm{Li}_{2.186}$	$d + 2\alpha$			
^{10}B	9.61 ± 0.06	240 ± 114	$d + {}^{6}\mathrm{Li}_{2.186}$	$d + 2\alpha$			
^{10}C	5.222 ± 0.004	294 ± 16	$p + {}^{9}\mathrm{B}_{g.s.}$	$2p + 2\alpha$	1000 ± 90	1010 ± 90	>0 (2^+)
^{10}C	6.553 ± 0.007[b]	214 ± 31	$p + {}^{9}\mathrm{B}_{g.s.}$	$2p + 2\alpha$	370 ± 33	540 ± 48[c]	>0
^{10}C	5.287 ± 0.005	106 ± 11	$2p + {}^{8}\mathrm{Be}_{g.s.}$	$2p + 2\alpha$	80.7 ± 7.2	97.1 ± 8.7[c]	
^{10}C	6.568 ± 0.011[b]	172 ± 31	$2p + {}^{8}\mathrm{Be}_{g.s.}$	$2p + 2\alpha$	71.9 ± 6.5	82.0 ± 7.4[c]	
^{10}C	6.56 ± 0.02	<380	$\alpha + {}^{6}\mathrm{Be}_{g.s.}$	$2p + 2\alpha$	<150	<130	
^{10}C	8.4 ± 0.1	~ 1000	$p + {}^{9}\mathrm{B}_{2.345}$	$2p + 2\alpha$			
^{13}N	13.65 ± 0.01	<300	$p + {}^{12}\mathrm{C}_{9.6}$	$p + 3\alpha$	82 ± 9	40 ± 7	
^{13}N	13.65 ± 0.01	<300	$\alpha + {}^{9}\mathrm{B}_{g.s.}$	$p + 3\alpha$	75 ± 10	56 ± 7	
^{13}N	16.6 ± 0.1	<350	$\alpha + {}^{9}\mathrm{B}_{2.345}$	$p + 3\alpha$			

[a]The errors quoted are statistical, in addition there is a ± 50 keV systematic error from the uncertainty in the energy calibration.

[b]The 6.553- and 6.568-MeV peaks are probably two decay branches of the same state.

[c]Some of the yields of these levels are associated with water contamination of the C target. We estimate that these cross sections should be reduced by roughly 20% to account for this.

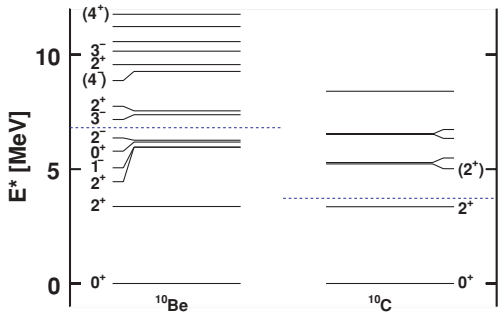

FIG. 1. (Color online) Level diagrams for the mirror nuclei ^{10}Be and ^{10}C. The dashed lines indicate the thresholds for particle decay.

resolution is channel dependent and increases with excitation energy. The resolution is dependent on target thickness, and the relative thicknesses of the Be and C targets were chosen to give the same predicted resolutions. For example, in the sequential two-proton decay of ^{10}C passing through the ^{9}B$_{g.s.}$ and ^{8}Be$_{g.s.}$ intermediate states, the predicted resolution (full width at half maximum, FWHM) increases from 130 keV at $E^* = 5$ MeV to 270 keV at $E^* = 7$ MeV.

A. ^{10}C decay

Below 15 MeV of excitation energy, the particle decay of ^{10}C excited states leads to the $2p + 2\alpha$ final state. As this is the only possible final state, it does not necessarily have strong selectivity for cluster structure. However, strong cluster structure in this nucleus is expected based on the mirror nucleus ^{10}Be [6]. The energy levels of the mirror nuclei are displayed in Fig. 1. The first excited 0^+ and 1^- states of ^{10}Be are proposed as bandheads for molecular configurations [17], and their mirror states in ^{10}C are particle unstable.

1. Excited states

Several decay paths leading to the $2p + 2\alpha$ channel can be isolated by selecting intermediate states populated in the decay of the excited ^{10}C nucleus [7,10]. Excitation-energy distributions for subsets of the $2p + 2\alpha$ events are shown in Fig. 2. Narrow peaks are observed in Figs. 2(a) and 2(b) corresponding to the ground states of ^{8}Be and ^{9}B from 2α and $p + 2\alpha$ correlations, respectively. For the latter case, there are two ways of choosing the proton from the $2p + 2\alpha$ event, and we have selected the one that gives the lowest ^{9}B excitation energy. Both of the ^{8}Be and ^{9}B peaks sit on negligible backgrounds and thus provide clean gates for the presence of these intermediate fragments.

The ^{10}C excitation-energy spectrum obtained by requiring an identified ^{9}B$_{g.s.}$ intermediate is displayed in Fig. 3(a). Results are shown for both the Be (curves) and C (data points) targets, and the Be results have been normalized to the same product of beam particles and target atoms per unit area. The results for the two targets are very similar showing two peaks at 5.22 and 6.55 MeV with the same yields. The widths of these peaks and other peaks of interest observed in this work are listed in Table I and were obtained from

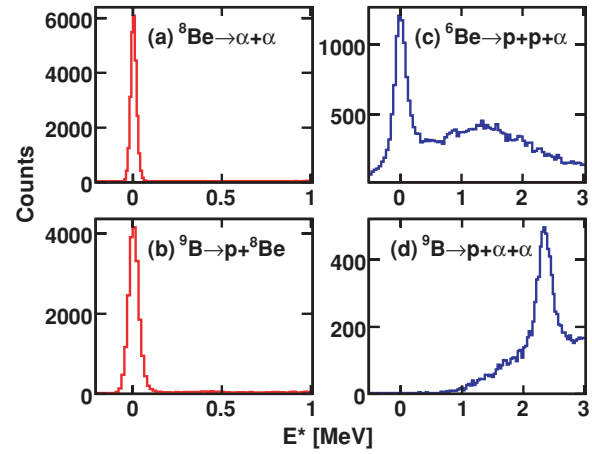

FIG. 2. (Color online) Experimental excitation-energy distributions of the indicated subevents in the $2p + 2\alpha$ exit channel. The results in (c) and (d) were obtained with a veto on the ^{8}Be$_{g.s.}$ peak in (a).

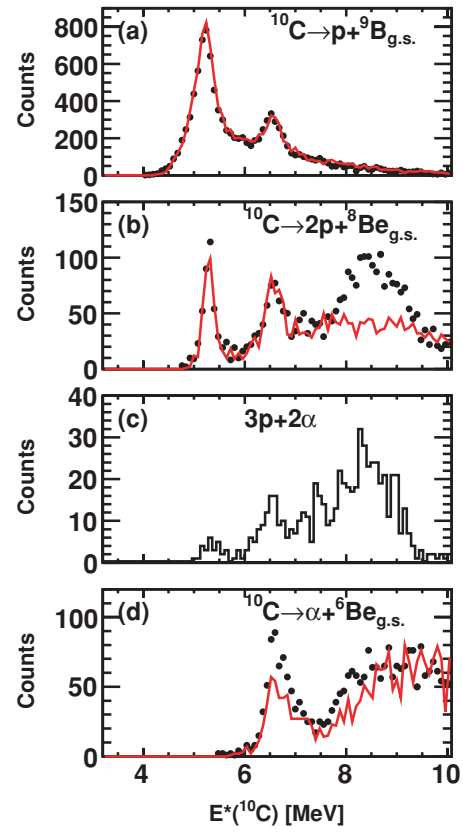

FIG. 3. (Color online) Comparison of experimental excitation-energy distributions obtained with the Be target (data points) and the C target (lines). The distributions are gated on (a) a ^{9}B$_{g.s.}$ intermediate, (b) a compound gate to select prompt two-proton emission, and (d) a ^{6}Be$_{g.s.}$ intermediate. The Be data have been normalized to the same product of beam atoms and target nuclei per unit area. The distribution shown in (c) was determined from $3p + 2\alpha$ events detected with the C target where one of the protons was ignored and the event was then analyzed with the same gating condition as used for distribution (b).

fitting Breit-Wigner lines shapes convoluted with the detector resolution as predicted with the Monte Carlo simulations. Cross sections are also listed which have been corrected for the simulated detector efficiency.

The 5.22- and 6.55-MeV peaks clearly correspond to sequential two-proton decay of ^{10}C through the ^{9}B$_{g.s.}$ to the ^{8}Be$_{g.s.}$. We also find evidence for prompt two-proton decay which bypasses the ^{9}B$_{g.s.}$ intermediate state. Figure 3(b) displays the excitation-energy distribution obtained by requiring a gate on an identified ^{8}Be$_{g.s.}$ and excluding the ^{9}B$_{g.s.}$ peak. With this event selection, we observe peaks at excitation energies of 5.29 and 6.57 MeV.

The broad peak at ~8.5 MeV in Fig. 3(b) obtained with the C target has been traced to interactions with hydrogen target nuclei from a water contamination of this target. A surprising number of $3p + 2\alpha$ events were detected with total energy and momentum consistent with interactions on hydrogen nuclei. If only two of the three protons from such events are detected, then these events will contaminate the $2p + 2\alpha$ channel. The contributions from this water contamination to the $2p + 2\alpha$ excitation-energy distributions were estimated by randomly throwing one of the three detected protons away and analyzing it as a $2p + 2\alpha$ event. The distribution obtained from these events with the same gating condition as in Fig. 3(b) is displayed in Fig. 3(c). This distribution also has a broad peak near $E^* = 8.5$ MeV, which suggests that these events are also the source of this feature in Fig. 3(b). In addition, there is some evidence for peaks at ~5.29 and ~6.57 MeV corresponding to the ^{10}C excited states observed in Fig. 3(b). Thus it appears that a fraction of the yield of these states is associated with interactions with hydrogen target nuclei. The cross sections σ_C in Table I have not been corrected for this effect, but we estimate that roughly 20% of the yields of these peaks are associated with the water contamination.

The peaks near $E^* \sim 6.56$ MeV in Figs. 3(a) and 3(b) probably correspond to the same state. The peak centroids and widths are consistent within the statistical errors (see Table I). Also, the relative yields of the two peaks are independent of which target was used.

Other decays that bypass the ^{8}Be ground state are indicated by the presence of intermediate states including the ^{6}Be$_{g.s.}$ and the $5/2^-$ 2.345-MeV excited state of ^{9}B, as shown in the $2p + \alpha$ and $p + 2\alpha$ correlations of Figs. 2(c) and 2(d), respectively.

For both of these excitation-energy distributions, we have excluded events in which the two α particles arise from ^{8}Be$_{g.s.}$ decay. A broad structure at $E^* = 8.4$ MeV is found to decay through the ^{9}B$_{2.345}$ intermediate level. The two-dimensional correlation between the ^{10}C and ^{9}B excitation energies for such events is displayed in Fig. 4. The excitation-energy spectrum for α-^{6}Be$_{g.s.}$ decay is plotted in Fig. 3(d), and shows an asymmetric peak for both targets at $E^* = 6.56 \pm 0.02$ MeV. This asymmetry may imply that this peak is a doublet, although the uncertain nature of the background makes the decomposition of such a doublet difficult. We list the width of the peak in Table I as <380 keV, where 380 keV is the width of the asymmetric peak with corrections for the resolution. If this peak is a doublet, then from the rising edge we estimate $\Gamma < 200$ keV for the main component. Also listed are limits

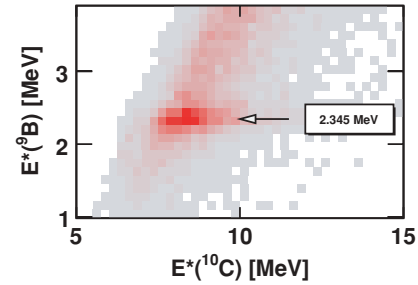

FIG. 4. (Color online) Three-particle ($\alpha\alpha p$) vs four-particle excitation energies showing a new state in ^{10}C at $E^* = 8.4$ MeV that decays through the 2.345-MeV state of ^{9}B.

for the cross section calculated by including the high-energy tails.

The mean energy of this peak is consistent within the statistical error with those observed near $E^* \sim 6.56$ MeV in Figs. 3(a) and 3(b). However, it seems that this peak is distinct from these in that there is a sizable dependence of the yield on the target in Fig. 3(d).

Based on the mirror nucleus ^{10}Be, we expect only two levels in the energy region around $E^* = 6.5$ MeV: a 2^+ and a 3^- state (Fig. 1). As we observed three peaks, it seems likely that at least two of them must be the separate decay branches of the same level. This suggests that a different nuclear structure is probed by the $\alpha + ^{6}$Be decay compared to decays to the ^{8}Be ground state, and that the peaks in Figs. 3(a) and 3(b) represent different decays of the same level, with branching ratios of $86 \pm 3\%$ for sequential proton decay, and $14 \pm 3\%$ for prompt two-proton decay.

2. *Correlations for sequential two-proton decay*

Further understanding of the structure of the observed states requires spin assignments. However, the spread in the beam energy was too large to isolate target excited states, making it difficult to deduce spin information from two-body scattering data. For the two levels that undergo sequential two-proton decay through the ^{9}B$_{g.s.}$ intermediate state, the distribution of relative angles θ_{pp} between the $^{10}\text{C} \rightarrow p + ^{9}\text{B}_{g.s.}$ and the $^{9}\text{B}_{g.s.} \rightarrow p + ^{8}\text{Be}_{g.s.}$ decay axes gives some information on the spins of these levels [18,19]. The experimental angular correlation for the 5.22-MeV state is shown as the data points in all panels of Fig. 5. Predicted correlations for assumed initial spins of $J = 0$–3 are displayed by the curves. These curves were obtained assuming a pure value for j, the total angular momentum removed by the proton in the first decay. The angular correlations are not sensitive to the parity of the initial state, even though different parities involve different values of the orbital angular momentum ℓ removed in the first decay. The predicted curves include the effects of the detector efficiency and resolution as modeled by the Monte Carlo simulations. To gauge the magnitude of the distortions introduced by the detector, the curves for $j = 1/2$ [Figs. 5(b) and 5(c)] correspond to uncorrelated decays, i.e., the primary distribution of the relative angle is isotropic, and thus the $\cos(\theta_{pp})$ distribution would be flat for a perfect detector.

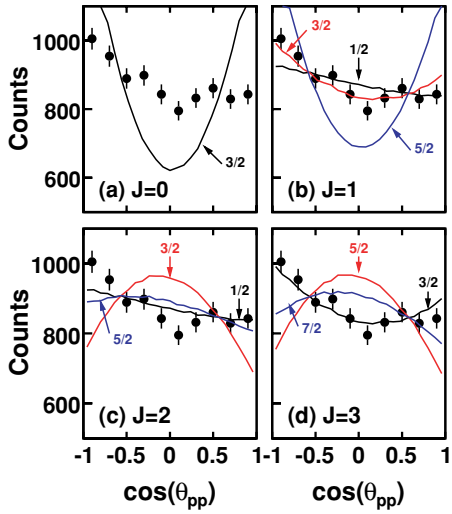

FIG. 5. (Color online) Experimental distribution of $\cos(\theta_{pp})$ for the 5.22-MeV state obtained with both the C and Be targets where θ_{pp} is the relative angle between the first two decay axes. This distribution is displayed in each panel and compared with predicted distributions for different assumed spins J of this state. The curves are labeled by the total angular momentum removed by the first emitted proton.

For $J = 0$, only a single j value is permitted, and the predicted correlations are clearly inconsistent with the data in Fig. 5(a). For other spins, multiple j values are possible, and only results for the lowest three values are shown. The curves for the larger values deviate strongly from the data. The best reproduction of the experimental data is obtained with $J = 1$, $j = 3/2$ and with $J = 3$, $j = 3/2$. In addition to the results for pure values of j, mixed j values are possible for which the predicted distribution contains a contribution from an interference term. Consider the decay of a $J = 2$ state with mixed $j = 1/2, 3/2$ values. The angular correlation is

$$w(\theta_{pp}) = |\alpha_{1/2}|^2 w_{1/2}(\theta_{pp}) + |\alpha_{3/2}|^2 w_{3/2}(\theta_{pp}) + (\alpha_{1/2}\alpha^*_{3/2} + \alpha^*_{1/2}\alpha_{3/2}) w_{\text{inter}}(\theta_{pp}), \quad (1)$$

where $w_{1/2}$ and $w_{3/2}$ are the correlations for pure $j = 1/2$ and 3/2 decay, $\alpha_{1/2}$ and $\alpha_{3/2}$ are their complex amplitudes, and w_{inter} is the interference term. With $|\alpha_{3/2}|^2/|a_{1/2}|^2 = 0.25$ and $(\alpha_{1/2}\alpha^*_{3/2} + \alpha^*_{1/2}\alpha_{3/2})/|\alpha_{1/2}|^2 = 1.0$, we obtain an identical dependence to the $J = 1$, $j = 3/2$ curve in Fig. 5(b) which fits the experimental data.

From a minimum χ^2-plus-one analysis, the data are consistent with $0.04 \leqslant |\alpha_{3/2}|^2/|\alpha_{1/2}|^2 \leqslant 0.83$ for $J = 2$. One can also consider mixing for the $J = 1$ case, where from a similar analysis we find very little mixing of $j = 1/2$ is allowed, i.e., $|\alpha_{1/2}|^2/|\alpha_{3/2}|^2 \leqslant 0.004$ at the 1σ level. In conclusion, from the angular correlation alone, we learn that the spin of this level is not $J = 0$, and different amounts of mixing are required for different assumed spins. This is summarized in Table II.

The 5.22-MeV level is expected to be the analog of either the 0^+, 1^-, 2^-, or 2^+ states in ^{10}Be, which are all separated from each other by less than 305 keV (Fig. 1). The values of j and ℓ of the first emitted proton consistent with these spin values are listed in Table III. Now a 0^+ state must be rejected as stated previously. For a 1^- state, the correlations imply that the first decay occurs predominantly by the emission of a $j = 3/2$, $\ell = 2$ proton. This would be surprising, as such a state could also decay by emitting a $j = 1/2$, $\ell = 0$ proton which has a lower centrifugal barrier. For a 2^- state, the correlations imply the first decay is a mixed $j = 1/2$, $\ell = 0$ and $j = 3/2$, $\ell = 2$ transition, whereas for a 2^+ state, this decay contains an admixture of $j = 1/2$, $\ell = 1$ and $j = 3/2$, $\ell = 1$ emission. The latter seems most likely, as we are mixing decays with the same centrifugal barriers. Thus of these possibilities, the assignment of 2^+ to this 5.22-MeV state is most likely.

TABLE II. Possible level spins J and angular momenta j removed by the first proton consistent with the angular correlations measured for the 5.22- and 6.55-MeV ^{10}C states.

J	j
5.22 MeV	
0	Not possible
1	$\frac{3}{2}$
2	Mixed $\frac{1}{2}$ and $\frac{3}{2}$
3	$\frac{3}{2}$
6.55 MeV	
0	Not possible
1	Mixed $\frac{1}{2}$ and $\frac{3}{2}$
2	$\frac{3}{2}$ possibly mixed with $\frac{1}{2}$
3	$\frac{5}{2}$ possibly mixed with $\frac{3}{2}$

In the database [14], ^{10}C levels are listed at 5.22 ± 0.04 and 5.38 ± 0.07 MeV, and it is stated that "one of these two states is presumably a 2^+ state." Evidence for a 2^+ state comes from the (^{3}He,t) reaction at $E^* = 5.28 \pm 0.06$ MeV [20]; from the (p,t) reaction at $E^* = 5.29 \pm 0.06$ MeV; and from the (p,n) reaction at 5.3 [21] and 5.2 ± 0.3 [22] MeV. In the present work, the state observed at 5.22 MeV is most likely this 2^+ state. The measured width is consistent (within uncertainties)

TABLE III. For each possible spin J^π of the 5.22- and 6.55-MeV ^{10}C states consistent with the mirror nucleus, the total and orbital angular momenta j and ℓ of the first emitted proton are listed which allow reproduction of the measured angular correlations.

J^π	(j, ℓ)
5.22 MeV	
$0+$	Not possible
1^-	$(\frac{3}{2}, 2)$
2^-	Mixed $(\frac{1}{2}, 0)$ and $(\frac{3}{2}, 2)$
2^+	Mixed $(\frac{1}{2}, 1)$ and $(\frac{1}{2}, 1)$
6.55 MeV	
2^+	$(\frac{3}{2}, 1)$ possibly mixed with $(\frac{1}{2}, 1)$
3^-	$(\frac{5}{2}, 2)$ possibly mixed with $(\frac{3}{2}, 2)$

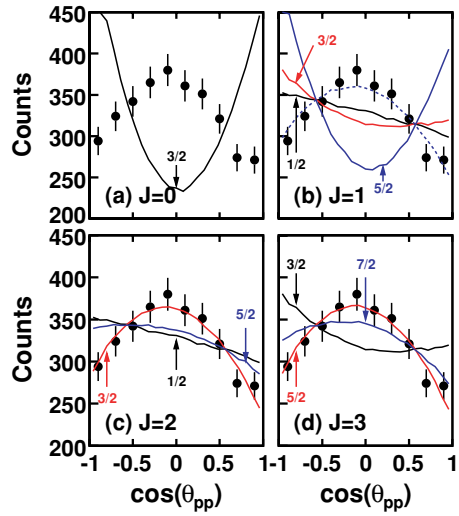

FIG. 6. (Color online) As for Fig. 5, but for the 6.56-MeV state. In addition, the dashed curve in (b) shows a distribution obtained with mixed $j = 1/2$ and 3/2 values with maximal interference.

with the value of 225 ± 45 keV listed in the database. This width and the location of the higher 5.38-MeV state come from the (^{3}He,t) study of Schneider *et al.* [23]. This higher level may be associated with our 5.29-MeV level, although the listed width of 300 ± 60 keV is much larger than the 106 ± 11 value of this work. However, this higher energy level was not resolved from the 5.22-MeV peak in Ref. [23], and the fitted width should be very sensitive to the assumed background.

Background-subtracted angular correlations for the 6.55-MeV state are shown in Fig. 6. These experimental correlations are stronger than those obtained for the 5.22-MeV state in Fig. 5. Again, the results are inconsistent with $J = 0$ as shown in Fig. 6(a). In Fig. 6(b), the $J = 1$ predictions with pure values of j are also inconsistent. A mixed $J = 1$ transition with $j = 1/2$ and 3/2 and $\alpha_{1/2} = -\alpha_{3/2}$ can reproduce the data [dashed line in Fig. 6(b)]. Based on the levels of the mirror nucleus ^{10}Be in Fig. 1, the 6.55-MeV state is expected to be either 2^+ or 3^-, making the $J = 1$ assignment less likely.

For the higher values of $J = 2$ and 3, one can also reproduce the data with pure $j = 3/2$ and 5/2 values, respectively, as shown in Figs. 6(c) and 6(d). Mixed j solutions are also possible. For $J = 2^+$, with a large interference term, considerable mixing of $j = 1/2$ and 3/2 decays (both $\ell = 1$) is consistent with the data as long as $|\alpha_{1/2}|^2/|\alpha_{3/2}|^2 < 2.25$. For $J = 3^-$, mixing is also possible between $j = 3/2$ and 5/2 decays both of which are also $\ell = 2$. We find $|\alpha_{3/2}|^2/|\alpha_{5/2}|^2 < 0.35$ is consistent with the experimental data. Combining the current results with expectations from ^{10}Be, it is most likely that this state has $J^\pi = 2^+$ or 3^-.

3. *Correlations for prompt two-proton decay*

The states at 5.29 and 6.57 MeV, which decay to the ^{8}Be$_{g.s.}$ without passing through the long-lived ^{9}B$_{g.s.}$ intermediate level, are examples of prompt two-proton emitters. These states are not "true" two-proton emitters in the sense of Goldansky [24], as there are ^{9}B intermediate states which are not energetically forbidden. In fact, for the 6.57-MeV peak, we have argued that it is a smaller decay branch of a state that decays mostly via sequential two-proton emission through the ^{9}B ground state. Possibly there is a minor sequential two-proton branch for the 5.29-MeV state that is not observed because it is obscured by the larger 5.22-MeV peak.

In addition, one may also consider a sequential decay scenario in which the emission of the first proton leaves the system in the first excited state of ^{9}B($E^* \sim 1.5$ MeV). However, as the lifetime of this intermediate state is so short ($\Gamma \sim 1.2$ MeV), the concept of sequential decay breaks down as the first proton will have traveled only an average distance of 4–5 fm before the second decay occurs. At the very least, final-state interactions between all three of the decay products ($2p + ^8$Be) should be considered. For the similar case of the two-proton decay of ^{6}Be$_{g.s.}$ where the ^{5}Li$_{g.s.}$ intermediate state is also short lived ($\Gamma = 1.23$ MeV), the correlations cannot be described by sequential decay but are reproduced by a three-body decay calculation [8,25].

The three-body decays are also interesting, as they probably represent prompt two-proton decay from cluster states. Of the possible ^{10}Be mirror states, we have assigned the 2^+ state to the 5.22-MeV peak. This leaves either the 0^+, 1^-, or 2^- states for the 5.29-MeV peak. In the mirror nucleus ^{10}Be, these states have been associated with a strong cluster structure, with the neutrons occupying the π molecular orbits for the 0^+ state and both the π and σ orbitals for the negative parity states [17]. The 0^+ state in particular is predicted to have a very strong deformation [26]. The 6.57-MeV state most likely has $J^\pi = 2^+$ or 3^-, both of which are expected to be higher members of the rotational bands built on the 0^+ or 1^- configurations, respectively [17].

The energy and angular correlations between the particles produced in the decay can be described by the hyperspherical Jacobi vectors $\mathbf{X}$ and $\mathbf{Y}$ and their conjugate momenta $\mathbf{k}_x$ and $\mathbf{k}_y$. There are two independent ways of defining the coordinates, which are referred to as the "T" and "Y" systems. These are illustrated in Fig. 7, where the core (fragment 3 in the T system or fragment 2 in the Y system) is the ^{8}Be$_{g.s.}$ fragment. In terms of the position vectors $\mathbf{r}_i$, momentum vectors $\mathbf{k}_i$, and masses

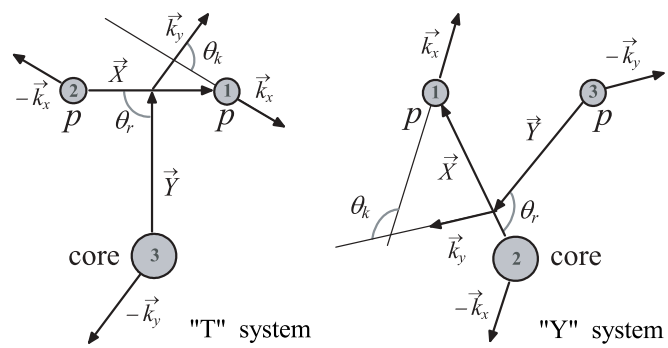

FIG. 7. Independent T and Y Jacobi systems for the core + N + N three-body system in coordinate and momentum spaces.

m_i ($i = 1$, 2, and 3), the Jacobi coordinates are

$$\mathbf{X} = \mathbf{r}_1 - \mathbf{r}_2\,, \tag{2a}$$

$$\mathbf{Y} = \frac{m_1\mathbf{r}_1 + m_2\mathbf{r}_2}{m_1 + m_2} - \mathbf{r}_3, \tag{2b}$$

$$\mathbf{k}_x = \frac{m_2\mathbf{k}_1 - m_1\mathbf{k}_2}{m_1 + m_2}\,, \tag{2c}$$

$$\mathbf{k}_y = \frac{m_3(\mathbf{k}_1 + \mathbf{k}_2) - (m_1 + m_2)\mathbf{k}_3}{m_1 + m_2 + m_3}. \tag{2d}$$

Of the six degrees of freedom required to define the $\mathbf{k}_x$ and $\mathbf{k}_y$ distributions, three describe the Euler rotation of the decay plane and one is constrained from energy conservation. Thus the complete correlation information can be described by two variables, which we take as E_x/E_T and θ_k, where E_x is the energy associated with the X coordinate,

$$E_x = \frac{(m_1 + m_2)k_x^2}{2m_1m_2}, \tag{3}$$

E_T is the total three-body energy, and θ_k is the angle between the Jacobi momenta,

$$\theta_k = \frac{\mathbf{k}_x \cdot \mathbf{k}_y}{k_x k_y}. \tag{4}$$

For each event, there are two ways of labeling the two protons, and thus there are two possible values of the $[E_x/E_T, \cos(\theta_k)]$ coordinate, both of which are used to increment the correlation histograms. For the T system, this produces a symmetrization of the angular distributions about $\cos(\theta_k) = 0$. The two-dimensional correlation pictures in both the T and Y system for the 5.29- and 6.57-MeV peaks are shown in Figs. 8 and 10, and the distributions projected on the angular and energy axes are illustrated in Figs. 9 and 11, respectively. The results for the 6.57-MeV peak were obtained after a background subtraction using the neighboring regions on either side of the peak to estimate the background. The correlations for the 5.29- and 6.57-MeV peaks have significant differences, which will be highlighted later.

To interpret the experimental correlations, it is useful to compare the data with the predictions of some idealized decay scenarios. In the first of these, called the "phase-space" scenario, the decay randomly samples the three-body phase space following the prescription of Ref. [27]. No further interactions between the fragments are considered.

In the second "sequential" scenario, the decay proceeds sequentially through the wide first excited state of ^{9}B. Again, we do not consider any further interactions between the fragments produced in the different decay steps. From the mirror nucleus ^{9}Be, the first excited state of ^{9}B is expected to have spin $1/2^+$, and thus a proton emission from this state to the $J = 0^+$ ^{8}Be ground state will be $\ell = 0$. Hence there should be no angular correlations between the two proton emission axes. The distribution of proton energies were taken from an R-matrix prescription given in Ref. [7].

Finally we model the decay as a "diproton" emission following the R-matrix prescription of Ref. [28]. As the diproton is $J = 0^+$, its decay axis has no preferred direction, and thus the $\cos(\theta_k)$ distribution in the T system should be flat. After the decay of the diproton, no interactions between the protons and the ^{8}Be fragment are considered. In all three scenarios, the effect of the detector bias and resolution are included via the Monte Carlo simulations.

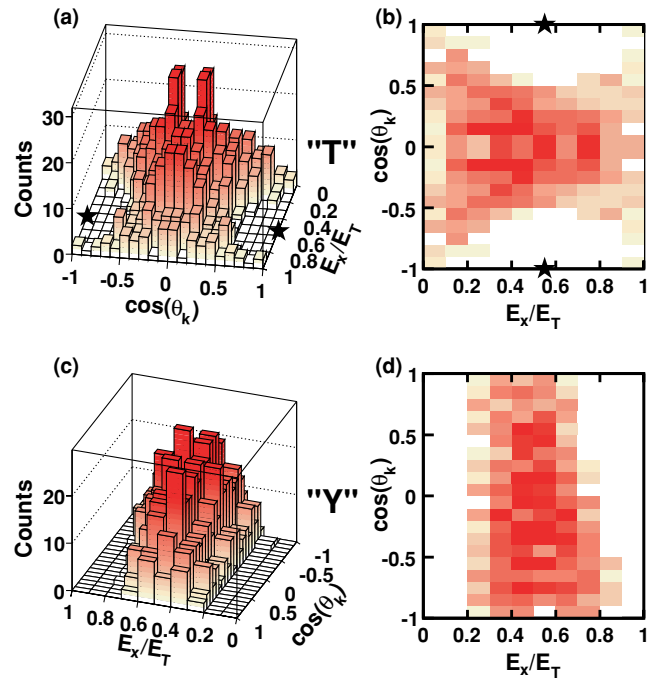

FIG. 8. (Color online) Full correlations in both the T and Y Jacobi systems for the 5.29-MeV state. In the T system, the star symbols indicate the coordinates at which the velocity vectors of the ^{8}Be intermediate and one of the protons are identical.

The predictions of the phase-space, sequential, and diproton scenarios are shown by the solid, dotted, and dashed curves, respectively, in Figs. 9 and 11. The full two-dimensional distributions in the T system are displayed in Fig. 12 for the 5.29-MeV peak, and the corresponding distributions for the 6.57-MeV state are qualitatively similar.

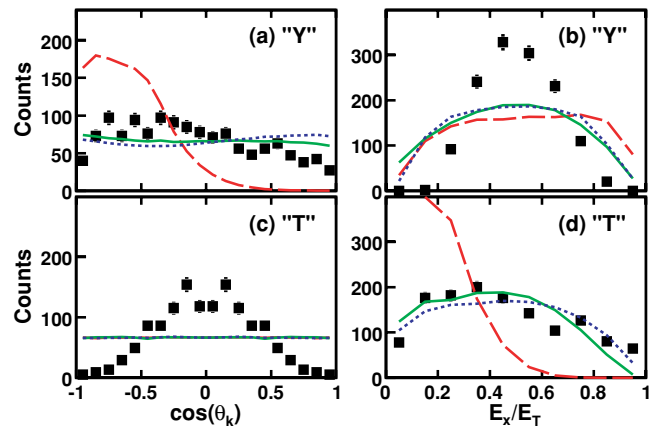

FIG. 9. (Color online) Projected correlations in both the T and Y Jacobi systems for the 5.29-MeV state. The solid, dotted, and dashed curves show the predictions of the phase-space, sequential, and diproton simulations, respectively, which include the effect of the detector bias and resolution via the Monte Carlo simulations. In (c) all three predictions are identical and thus the curves are not separated.

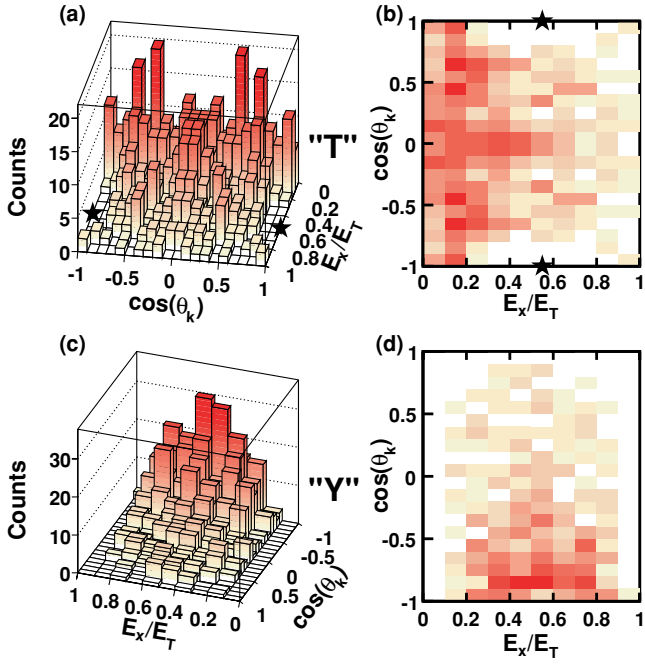

FIG. 10. (Color online) Same as Fig. 8, but for the 6.57-MeV state.

Let us start by concentrating on the results for the 5.29-MeV peak. The sequential and phase-space predictions are quite similar, and there is reasonable agreement between the data and these two predictions for the energy distribution in the T system [Fig. 9(d)] and, to a lesser extent, the angular distribution in the Y system [Fig. 9(a)]. However, the agreement between theory and experiment for the other distributions is much poorer. The diproton predictions are clearly inconsistent with all the projected experimental distributions in Fig. 9.

These comparisons indicate that the decay of the 5.29-MeV state is more complex than these idealized scenarios. For instance, the presence of strong Coulomb interactions are manifested in the experimental correlations. The ^{8}Be core and one of the protons have the same velocity vectors when $\cos(\theta_k) = \pm 1$ and $E_x/E_T = 0.545$ in the T system. These

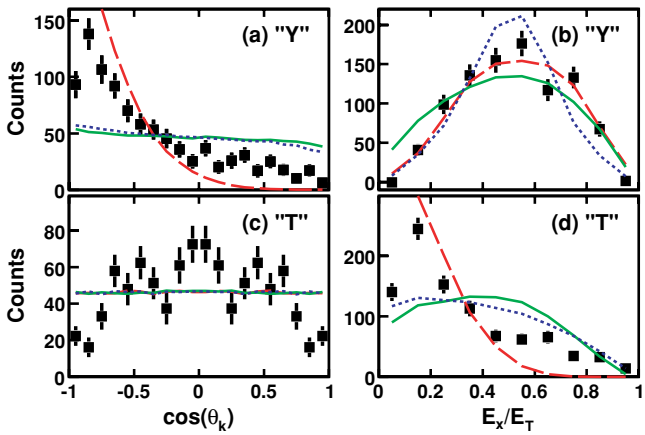

FIG. 11. (Color online) Same as Fig. 9, but for the 6.57-MeV state.

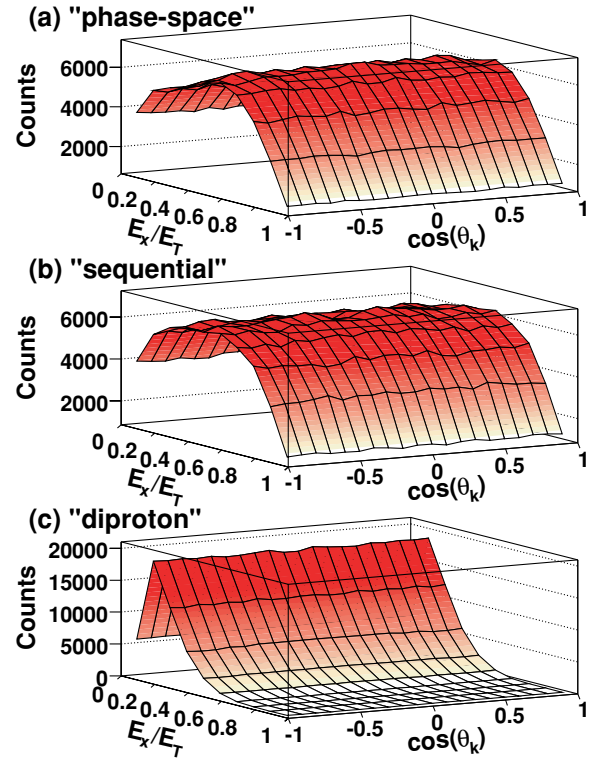

FIG. 12. (Color online) Predicted full correlations in the Jacobi T system for the three decay simulations. These predictions take into account the effect of the detector bias and resolution via the Monte Carlo simulations.

points are indicated in Figs. 8(a) and 8(b) by the star symbols. In the regions of the T plot surrounding these points, there is a clear suppression of events, which can be attributed to Coulomb interactions between this proton and the core. In the Y system, the corresponding conditions are $E_x/E_T = 0$ and $E_x/E_T = 1$, the regions bordering the two-dimensional plot in Fig. 8(d). Again we see a suppression of events in these regions due to Coulomb interactions. Of course in our idealized phase-space, sequential, and diproton predictions in Fig. 12, this effect is absent, as the simulations did not include these interactions.

Similar Coulomb effects are also seen in the experimental correlations for ^{6}Be$_{g.s.}$ and ^{45}Fe$_{g.s.}$ decay in Refs. [29,30]. Overall, the correlations for the 5.29-MeV peak are intermediate between these two cases. To illustrate this, a comparison of experimental angular distributions in the T system and energy distributions in the Y system for ^{6}Be, ^{10}C, and ^{45}Fe are made in Fig. 13. For the energy distributions in the Y system, the Coulomb interactions suppress the edges of the distributions ($E_x/E_T = 0, 1$) and thus cause a bunching of the yield in the center.

Goldansky assumed that the probability for simultaneous subbarrier emission of two protons is governed by the product of the barrier penetration factors for each of the two protons [24]. This probability is maximized when the two protons have the same energy, and thus equal energy protons are expected on average, and the more subbarrier the emissions, the narrower the distribution of the proton energies about this

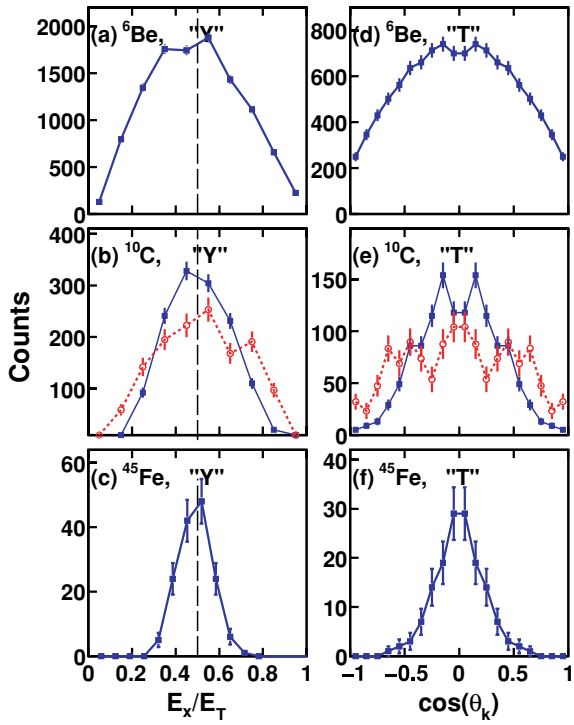

FIG. 13. (Color online) Comparison of experimental angular distributions in the T systems and energy distributions in the Y systems for ^{6}Be$_{g.s.}$ [8], ^{10}C, and ^{45}Fe$_{g.s.}$ [30] decay. For ^{10}C, results are shown for the 5.29-MeV (solid lines) and the 6.57-MeV (dotted lines) states.

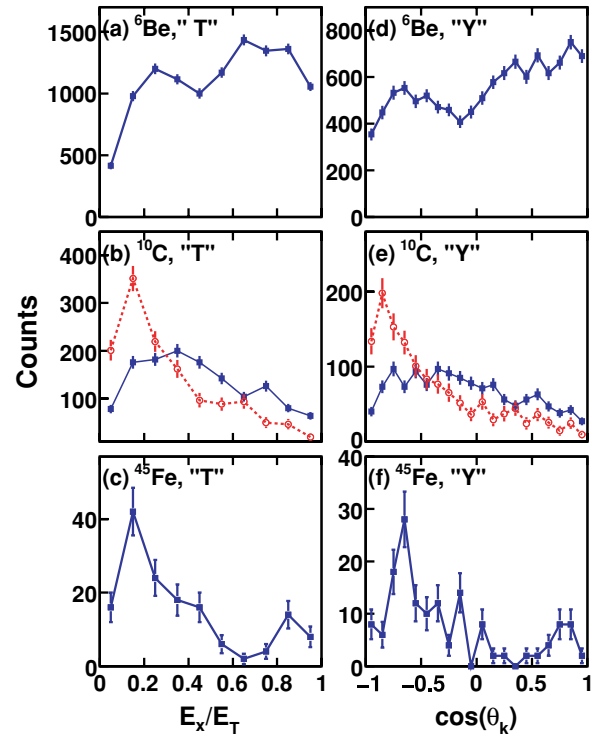

FIG. 14. (Color online) Comparison of experimental energy distributions in the T systems and angular distributions in the Y system for ^{6}Be$_{g.s.}$ [8], ^{10}C, and ^{45}Fe$_{g.s.}$ [30] decay. For ^{10}C, results are shown for the 5.29-MeV (solid lines) and the 6.57-MeV (dotted lines) states.

average. Predictions from the three-body cluster decay model [31] are consistent with these expectations giving narrower energy distributions in the Y system with increasing Z of the nucleus.

If the two equal-energy protons are emitted in a diproton configuration, i.e., at the same angle, then in the Y system,

$$\frac{E_x}{E_T} = \frac{1}{2} + \frac{1}{2(A_{\text{core}}+1)} > \frac{1}{2}, \tag{5}$$

whereas if they are emitted in opposite directions,

$$\frac{E_x}{E_T} = \frac{1}{2} - \frac{1}{2(A_{\text{core}}+1)} < \frac{1}{2}, \tag{6}$$

where A_{core} is the mass number of the core. These equations only differ by the sign of the second term; back-to-back configurations give values less than $\frac{1}{2}$ and diproton configurations give values greater than $\frac{1}{2}$. For heavy systems, the second term is negligible, and thus only for light systems do we expect the centroid of the energy distributions in the Y system to be displaced significantly from the value $\frac{1}{2}$. This is most clearly seen for the ^{6}Be system where the centroid is 0.491 ± 0.003, indicating that back-to-back emissions are somewhat more probable than diproton-like emissions. This observation is also consistent with the angular distribution in the Y system [Fig. 14(d)], which is skewed toward positive cos(θ_k) values.

Comparisons between the experimental energy distributions in the T system and angular distributions in the Y system for the three nuclei are made in Fig. 14. For each system, the corresponding angular and energy distributions all have the same shape and thus contain similar information about the nuclear structure. In core-p-p cluster calculations [8], these distributions were found to have the largest dependence on the assumed core-p interaction.

The energy-angular correlations for the 6.57-MeV peak are quite different from those obtained for the 5.29-MeV peak. The phase-space and sequential simulations in this case do not give a reasonable description of the energy distribution in the T system [Fig. 11(d)] and the angular distribution in the Y system [Fig. 11(a)]. In contrast, the diproton simulation reproduces the strong enhancement for small relative energies between the protons which is visible in the T energy distribution of Fig. 11(d). This simulation also correctly reproduces the strong enhancement on the Y angular distribution of Fig. 11(a) near $\cos(\theta_K) = -1$. Both of these features were missing in the experimental 5.29-MeV results.

Diproton emission should give an isotropic angular distribution in the T system. In Figs. 13(d)–13(f), a comparison of the angular distributions for ^{6}Be, ^{10}C, and ^{45}Fe two-proton decays indicates that the 6.57-MeV case is by far the most isotropic. Comparisons of the energy distribution in the Y systems for the two ^{10}C states in Fig. 13(b) confirms that the 6.57-MeV state has a larger width consistent with the reduced subbarrier nature of its decay.

The measured correlations thus suggest that the prompt two-proton decay of the 6.57-MeV state has a strong

diproton character. However, there are features of the data not reproduced by the simple diproton model. The Coulomb suppressions observed for the lower energy state are also present for the 6.57-MeV state, albeit at a reduced level. The full correlation plots in Figs. 10(a) and 10(b) again show a suppression of events in the neighborhood of the star symbols. This smaller suppression is not surprising, as the fragment momenta are larger for the 6.57-MeV state reducing the effect of Coulomb repulsion. The reduced magnitude of this Coulomb suppression is also manifest in the wider energy distribution in the Y system. See Fig. 13(b) for a comparison of this distribution for the 5.29- and 6.57-MeV states.

4. Other $2p + 2\alpha$ studies

Curtis *et al.* [32] have also studied ^{10}C excited states through the detection of $2p + 2\alpha$ events following the inelastic scattering of ^{10}C beams from a C target. The main difference from the present work is the higher beam energy of $E/A = 30$ MeV. Several similarities and differences exist between the current results and those of Curtis *et al.* They observed a state at $E^* = 5.31$ MeV decaying to $p + {}^9\mathrm{B}_{\mathrm{g.s.}}$ as well as a 6.74-MeV level decaying to $\alpha + {}^6\mathrm{Be}_{\mathrm{g.s.}}$, similar to our 5.22- and 6.56-MeV peaks.

Neither the 6.55- nor the 6.57-MeV peak associated with sequential and correlated two-proton decay was observed by Curtis *et al.* If all the ∼6.56-MeV structures listed in Table I are branches of the same state, then Curtis *et al.* should have observed it. From the cross sections listed in Table I, the branching ratio for the prompt two-proton branch would be comparable to or larger than that for $\alpha + {}^6$Be, and the sequential two-proton branch would have a much larger yield. Given that the lower energy 5.31-MeV sequential two-proton state is clearly observed in the work of Curtis *et al.*, it seems unlikely these higher energy peaks would have been missed. Therefore their absence in the data of Curtis *et al.* implies that the 6.56-MeV $\alpha + {}^6$Be peak is a state distinct from the 6.55-MeV two-proton-decay peaks.

Another difference between the two studies is that Curtis *et al.* did not observe the 5.29-MeV peak associated with prompt two-proton decay. However, they do report a peak at 4.2 MeV for $p + {}^9\mathrm{B}_{\mathrm{g.s.}}$ decay which they assign $J^\pi = 0^+$, but it does not appear in our data. Our simulated efficiency for the detection of such a state is 4%, comparable to the value obtained at $E^* = 5.22$ MeV, and if such a level had been excited in the present study it should have been observed. From a theoretical point of view, Fortune and Sherr [33] and Barker [34] argue that the 0^+ state should be above $E^* = 5.0$, thus questioning the validity and/or the spin assignment of this peak.

Curtis *et al.* indicated that this purported 4.2-MeV state undergoes sequential two-proton decay through the $^9\mathrm{B}_{\mathrm{g.s.}}$; thus from the predictions in Figs. 5(a) and 6(a), it is clear that there should be strong angular correlations between the protons if it is indeed a 0^+ state. Thus the data of Curtis *et al.* could be used to test this and determine the validity of this peak and its spin assignment.

B. ^{9}B decay

The ground and excited states of ^{9}B decay to the $p + 2\alpha$ exit channel. The 2.345-MeV $J = 5/2^-$ state of ^{9}B is unusual, as it is one of the few low-lying ^{9}B states that do not decay predominantly through the ^{8}Be ground state. Instead it is listed as decaying 99.5% of the time by α emission to the unstable ^{5}Li ground state [14]. This branching ratio comes from Ref. [35], where the remaining 0.5% branch associated with $p + {}^8\mathrm{Be}_{\mathrm{g.s.}}$ decay was also measured. However for the main branch, they could not differentiate between $\alpha + {}^5\mathrm{Li}_{\mathrm{g.s.}}$ decay and proton decay to the $E^* = 3.03$ MeV, $J = 2^+$ first excited state of ^{8}Be.

The mirror state in ^{9}Be at 2.429 MeV is also reported to decay by α emission in Ref. [14]. In this case, it would decay to the unstable ^{5}He ground state producing the $n + 2\alpha$ final state. However, in some recent experiment work, Papka *et al.* claim that this state decays almost exclusively by n emission to the unstable first excited state of ^{8}Be [36]. The decay mechanism is of interest for deducing the $\alpha + \alpha + n$ reaction rate in high-energy and neutron-rich astrophysical environments [37,38].

As protons can be detected more easily and with better resolution that neutrons, it is useful to look closely at the correlations in the present data from the $^9\mathrm{B}(5/2^-)$ state to determine the contributions from $\alpha + {}^5\mathrm{Li}_{\mathrm{g.s.}}$ and $p + {}^8\mathrm{Be}_{2^+}$ decay. Although the decays of these mirror states have been described as sequential, in reality the $^5\mathrm{He}_{\mathrm{g.s.}}$, $^5\mathrm{Li}_{\mathrm{g.s.}}$, and $^8\mathrm{Be}_{2^+}$ intermediate states are all very short-lived with decay widths of 0.648, 1.23, and 1.513 MeV, respectively, and thus these decays are more correctly described as three-body in nature.

To study this issue, an analysis was performed starting with events where two α particles and a proton were detected. Those events in which the two α-particle velocity vectors were consistent with $^8\mathrm{Be}_{\mathrm{g.s.}}$ decay were discarded, thus eliminating all low-lying ^{9}B excited states except for the one at 2.345 MeV. The reconstructed ^{9}B excitation-energy distribution is shown in Fig. 15 and is very similar in shape to the spectrum in Fig. 2(d) obtained from ^{9}B fragments formed after proton decay of ^{10}C excited states. However, the yield from the $p + 2\alpha$ events is significantly larger here than that obtained in Fig. 2(d). Many of the 2.345-MeV events from the $p + 2\alpha$ analysis likely arise from ^{10}C decays in which one of the protons was not detected. In addition, we expect contributions from ^{9}B projectile-like fragments formed after proton transfer to the target. Adjacent regions on each side of the peak were used for background subtraction in the correlation analysis.

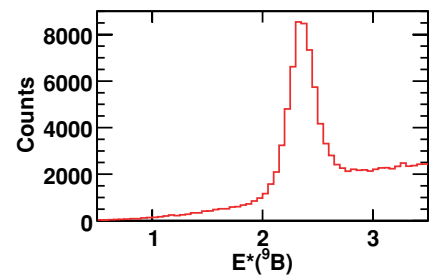

FIG. 15. (Color online) Excitation-energy distribution of ^{9}B fragments obtain from the $p + 2\alpha$ events where the two α particles are not associated with $^8\mathrm{Be}_{\mathrm{g.s.}}$ decay.

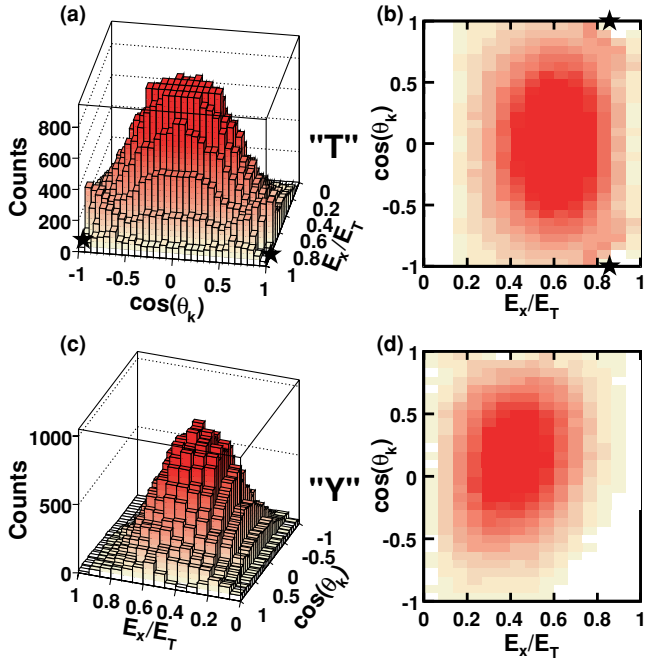

FIG. 16. (Color online) Full correlation plots in both the T and Y Jacobi systems for the decay of the 2.345-MeV state of ^{9}B. In the T system, the star symbols indicate the coordinates at which the velocity vectors of the proton and one of the α particles are identical.

As before, the correlations are presented using the Jacobi T and Y coordinate systems except with a different labeling convention: particle 3 in the T system and particle 2 in the Y system, both labeled as the core in Fig. 7, now refer to the proton. The remaining labels refer to the α particles. Thus E_x in the T system is now the relative energy between the two α particles. Full correlation plots are displayed in Fig. 16, and the projections on the energy and angular axes are shown in Fig. 17.

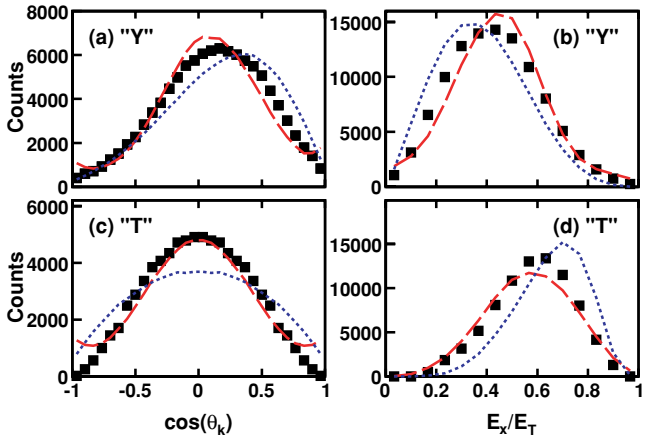

FIG. 17. (Color online) Projected correlation plots in both the T and Y Jacobi systems for the 2.345-MeV state of ^{9}B. The dashed and dotted curves show the predictions of sequential $\alpha + {}^{5}\mathrm{Li}_{\mathrm{g.s.}}$ and $p + {}^{8}\mathrm{Be}_{2^+}$ decay simulations including the effects of the detector resolution and efficiency.

Simulations of sequential ^{9}B decay through the $^{5}\mathrm{Li}_{\mathrm{g.s.}}$ and $^{8}\mathrm{Be}_{2^+}$ intermediate states were performed. As before, no final-state interactions between the fragments were considered. The total kinetic energy E_T is subdivided into E_1 and E_2, the contributions emitted in the first and second decay steps, respectively ($E_1 + E_2 = E_T$). The distribution of E_1 is determined as

$$f(E_1) \propto P_{\ell_1}(E_1) \frac{\Gamma_{\ell_2}(E_2)}{[E_2 - E_r - \Delta_{\ell_2}(E_2)]^2 + [\Gamma_{\ell_2}(E_2)/2]^2}, \tag{7}$$

where the first factor is the penetrability factor for the emission of the first particle with orbital angular momentum ℓ_1 calculated from Ref. [39] with the channel radius $1.4(A_1^{1/3} + A_2^{1/3})$. The second factor is the R-matrix description of the line shape of the intermediate state [39], where E_r is its resonance energy,

$$\Gamma_{\ell_2}(E_2) = 2\gamma_{\ell_2}^2 P_{\ell_2}(E_2), \tag{8}$$

$$\Delta_{\ell_2}(E_2) = -\gamma_{\ell_2}^2 [S_{\ell_2}(E_2) - B], \tag{9}$$

ℓ_2 is the orbital angular momentum of the second decay, $\gamma_{\ell_2}^2$ is the reduced width of the intermediate state, B is the boundary condition, and S_{ℓ_2} is the shift function. The line shapes of the ^{5}Li and $^{8}\mathrm{Be}_{2^+}$ are asymmetric, and the R-matrix parameters E_r, $\gamma_{\ell_2}^2$, and B were taken from Refs. [40] and [41], respectively. The predicted distribution functions for E_1 are displayed in Fig. 18(a).

For α decay to $^{5}\mathrm{Li}_{\mathrm{g.s.}}$, $j_1 = \ell_1 = 2$ and the angular correlation in the ^{9}B frame between the two decay axes is

$$w_2(\theta_{12}) = \frac{35 - 18\cos(2\theta_{12}) + 15\cos(4\theta_{12})}{160\pi}. \tag{10}$$

The angle θ_{12} is identical to θ_k in the Jacobi T system for this decay. The distribution is normalized such that

$$2\pi \int_0^{\pi} w_2(\theta_{12}) \sin(\theta_{12})\, d\theta_{12} = 1, \tag{11}$$

and it is displayed as the solid curve in Fig. 18(b).

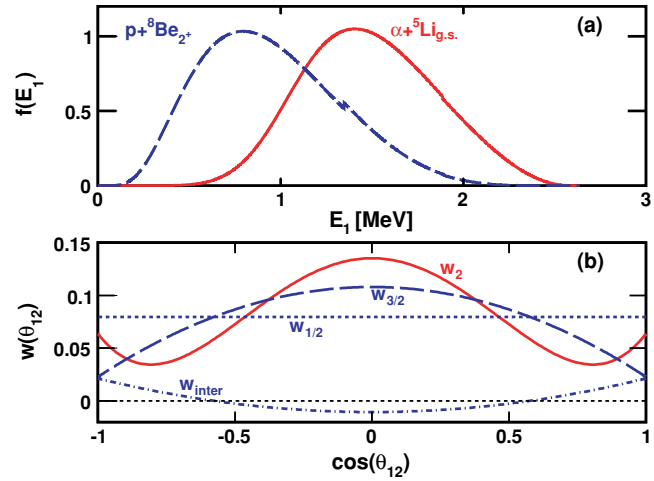

FIG. 18. (Color online) (a) Distribution of E_1, the energy released in the first step of the sequential decay of the $^{9}\mathrm{B}_{2.345}$ state, for the two decay simulations. (b) Sequential-decay angular correlations discussed in the text.

For $p + {}^{8}\mathrm{Be}_{2^+}$ decay, $\ell_1 = 1$ and $j_1 = 1/2$ and/or 3/2 and thus there is no unique angular correlation to use for this simulation. Possible correlations can be obtained from Eq. (1) where now

$$w_{1/2}(\theta_{12}) = \frac{1}{4\pi}, \tag{12}$$

$$w_{3/2}(\theta_{12}) = \frac{23 - 15\cos(2\theta_{12})}{112\pi}, \tag{13}$$

$$w_{\mathrm{inter}}(\theta_{12}) = \frac{1 + 3\cos(2\theta_{12})}{16\sqrt{14}\pi}. \tag{14}$$

These angular correlations are displayed in Fig. 18(b). The possible correlations range from isotropic ($w_{1/2}$) to a moderate enhancement at $\theta_{12} = 90^\circ$. The experimental correlations in Fig. 17(c) have a large ratio $w(\theta_{12} = 90^\circ)/w(\theta_{12} \sim 0^\circ, 180^\circ)$. To reproduce this behavior, we choose $\alpha_{1/2} = -0.333\alpha_{3/2}$ which maximizes that ratio in the $p + {}^{8}\mathrm{Be}_{2^+}$ simulations.

The simulated correlations in the Jacobi T system are displayed Fig. 19 and the projections are compared with the experimental data in Fig. 17. For $p + {}^{8}\mathrm{Be}_{2^+}$ decay, although the α coefficients were chosen to maximize the yield at $\theta_{12} = 90^\circ$ in Fig. 17(c), it was insufficient to reproduce the data. The predictions of this simulation also fail for the energy distributions in Figs. 17(b) and 17(d).

On the other hand, the $\alpha + {}^{5}\mathrm{Li}_{\mathrm{g.s.}}$ decay simulation reproduces the experimental data quite well, except that it predicts wings or enhancements near $\theta_{12} = 0^\circ, 180^\circ$ in the angular distribution in the both the T and Y systems [Figs. 17(a) and 17(c)] that can be traced to the w_2 angular correlation in Fig. 18(b). These features are not present in the data. At these angles, one of the fragments produced in the second step of the simulation is directed toward the first emitted α particle. Such events would be strongly suppressed by Coulomb final-state interactions.

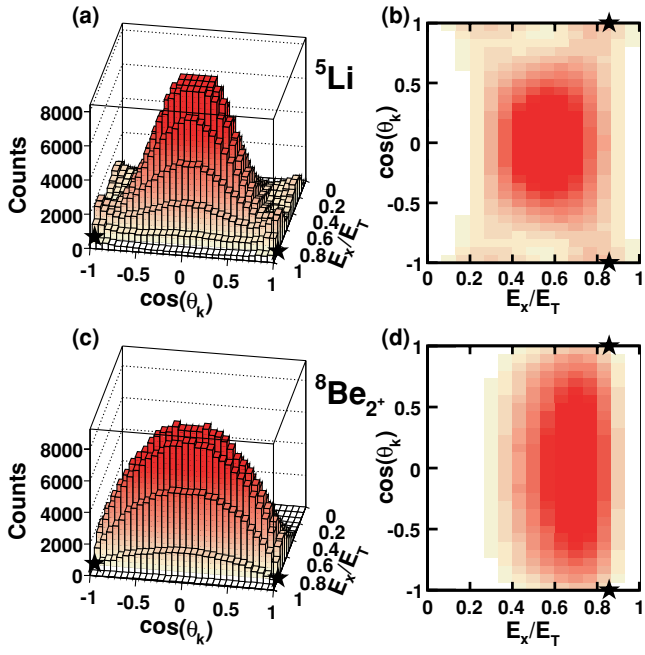

FIG. 19. (Color online) Simulated correlations in the Jacobi T system for $\alpha + {}^{5}\mathrm{Li}_{\mathrm{g.s.}}$ decay and $p + {}^{8}\mathrm{Be}_{2^+}$ decay. The star symbols indicate the coordinates at which the velocity vectors of the proton and one of the α particle are identical.

This result suggests that despite the large ${}^{5}\mathrm{Li}_{\mathrm{g.s.}}$ width, the decay of the 2.345-MeV state still has a strong $\alpha + {}^{5}\mathrm{Li}_{\mathrm{g.s.}}$ sequential character. The corresponding mirror state in ^{9}Be would be expected to decay through the mirror channel $\alpha + {}^{5}\mathrm{He}_{\mathrm{g.s.}}$, instead of through the $n + {}^{8}\mathrm{Be}_{2^+}$ channel as reported by Papka *et al.* [36]. In addition, we note that although R-matrix calculations of the ${}^{9}\mathrm{B}(5/2^-)$ sequential decay predict $\alpha + {}^{5}\mathrm{Li}_{\mathrm{g.s.}}$ as the dominant channel, they significantly underestimate the total decay width by a factor of 4 or more [42]. Clearly a three-body decay theory is needed for a full description of this state.

C. ^{10}B decay

Excited ^{10}B fragments were created in (p,n) exchange reactions and possibly more complex processes. Excited states were observed in three exit channels: $\alpha + {}^{6}\mathrm{Li}_{\mathrm{g.s.}}$, $p + {}^{9}\mathrm{Be}_{\mathrm{g.s.}}$, and $d + 2\alpha$. The $d + 2\alpha$ events contain contributions from the decay of both ${}^{8}\mathrm{Be}_{\mathrm{g.s.}}$ intermediates and the $E^* = 2.186$ MeV 3^+ state of ^{6}Li as indicated in the α-α and d-α correlations displayed in Fig. 20. Excitation-energy distributions gated on the different decay paths are shown in Fig. 21.

The results of this work are similar to those of Leask *et al.* [43], who observed the same ^{10}B decay channels following the ${}^{7}\mathrm{Li}({}^{12}\mathrm{C},{}^{10}\mathrm{B}^*){}^{9}\mathrm{Be}$ reaction. In this work, we have more events but poorer excitation-energy resolution. The $\alpha + {}^{6}\mathrm{Li}_{\mathrm{g.s.}}$ excitation-energy distribution, shown in Fig. 21(a), is similar to the spectrum reported by Leask *et al.* The arrows in Fig. 21(a) indicate the energies of states that are strongly populated in $\alpha + {}^{6}\mathrm{Li}_{\mathrm{g.s.}}$ reactions and that were assigned to these peaks by Leask *et al*. The first peak is associated with the 4.774-MeV 3^+ level. while the second peak may contain contributions from both the 5.11-MeV 2^- and 5.182-MeV 1^+ levels. For the third peak, three levels (5.92-MeV 2^+, 6.02-MeV 4^+, and 6.13-MeV 3^-) may contribute, while the forth peak can be associated with the 6.56-MeV state.

Of the channels observed, the $p + {}^{9}\mathrm{Be}_{\mathrm{g.s.}}$ is the only channel consistent with isospin $T = 1$. Therefore, it is not surprising that the peaks observed for the $p + {}^{9}\mathrm{Be}_{\mathrm{g.s.}}$ channel in Fig. 21(b) have strong $T = 1$ contributions. The arrows in this figure indicate known states with $T = 1$ and with mixed $T = (0 + 1)$ contributions. Most prominent are peaks at $E^* = 7.4$

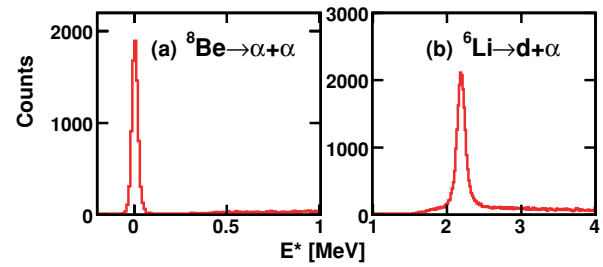

FIG. 20. (Color online) Excitation-energy distributions for the indicated subevents obtained for the $d + 2\alpha$ exit channel with both the Be and C targets.

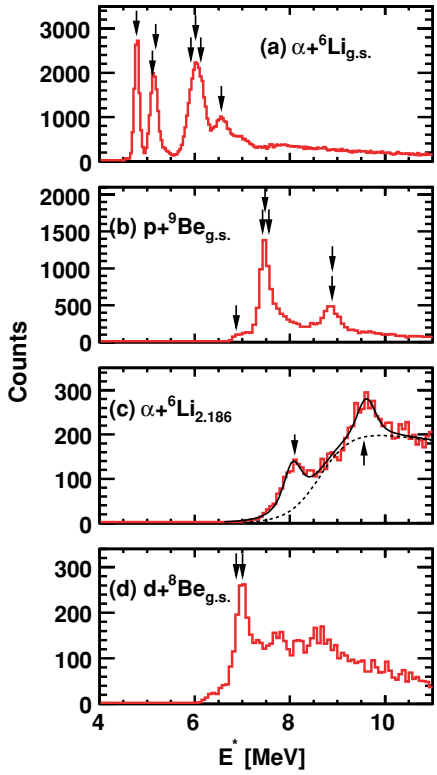

FIG. 21. (Color online) Excitation-energy distributions for ^{10}B nuclei determined for the indicated decay paths with both the C and Be targets. The arrows indicate the locations of previously known narrow states. In (c), the solid curve is a fit to the distribution used to extract the peak widths; the dashed curve shows the fitted background.

and 8.9 MeV. The former may contain contributions from 7.428-MeV $J = 1^- T = (0 + 1)$, 7.479-MeV $J = 2^- T = 1$, and 7.559-MeV $J = 0^+ T = 1$ levels, while the latter is maybe a doublet of the known $E^* = 8.887$-MeV $J = 3^-$ and 8.895-MeV $J = 2^+ T = 1$ states. In addition to the peaks, there is a low-energy shoulder, which probably corresponds to the 6.875-MeV $J = 1^- T = (0 + 1)$ level, the partner to the other mixed isospin level associated with the state at $E^*(^9\mathrm{B}) = 7.428$ MeV.

Excitation-energy distributions for the two decay paths associated with the $d + 2\alpha$ channel are shown in Figs. 21(c) and 21(d). A 7.00-MeV peak appears in coincidence with both the $^8\mathrm{Be}_{g.s.}$ and $^6\mathrm{Li}_{2.118}$ excited state. For the latter case, we found that the angular correlations between the purported decay steps were strongly asymmetric about $\cos\theta = 0$ and not consistent with sequential decay through the $^6\mathrm{Li}_{2.186}$ state. To remove these events from the $\alpha + {}^6\mathrm{Li}_{2.186}$ distribution in Fig. 21(c), we applied the extra condition that the α-α correlation was not consistent with $^8\mathrm{Be}_{g.s.}$ decay. The $\alpha + {}^6\mathrm{Li}_{2.186}$ distribution shows two broad peaks which were fit with two Breit-Wigner line shapes convoluted with the predicted energy-dependent detector resolution. From the fit, indicated by the solid curve in Fig. 21(c), we extract the level parameters $E^* = 8.06 \pm 0.05$ MeV ($\Gamma = 379 \pm 50$ keV) and $E^* = 9.62 \pm 0.06$ ($\Gamma = 240 \pm 114$ keV). The large uncertainty in the widths are due to the uncertainty in the background under these peaks (dashed curve). States at similar energies were observed by Leask *et al.* for which the consistent values of $E^* = 7.96 \pm 0.07$ ($\Gamma = 285 \pm 91$ keV) and 9.58 ± 0.06 MeV ($\Gamma = 257 \pm 64$ keV) were obtained. A peak at 7 MeV dominates the $d + {}^8\mathrm{Be}_{g.s.}$ distribution in Fig. 21(d). This peak is consistent with the 7.004-MeV $J = 3^-$ state.

D. ^{13}N decay

Evidence for states in ^{13}N is seen in the four-body final state $p + 3\alpha$. An important source of these events appears to be α transfer reactions creating ^{14}O fragments that proton decay to ^{13}N. The evidence for ^{14}O fragments comes from the surprising number of $2p + 3\alpha$ events detected given the low detection efficiency expected for this five-body channel.

The excitation-energy distributions from particle pairs and triplets of subevents shown in Fig. 22 suggest several intermediate states: $^8\mathrm{Be}_{g.s.}$, the ground and $5/2^-$, 2.345-MeV states of ^{9}B, and the 0^+ (7.65 MeV) and 3^- (9.64 MeV) excited states of ^{12}C. The ^{13}N excitation-energy spectra obtained after selecting different intermediate states are shown in Fig. 23. A 13.65-MeV state is prominent in both the $\alpha + {}^9\mathrm{B}_{g.s.}$ [Fig. 23(a)] and the $p + {}^{12}\mathrm{C}_{9.64}$ [Fig. 23(c)] channels. These peaks have FWHM of approximately 420 keV, which is the predicted experimental resolution. These peaks could therefore be intrinsically quite narrow; however, from the statistical errors associated with the experimental widths, we obtain a limit of 300 keV for the intrinsic width. Using efficiencies determined with the Monte Carlo simulations, the branching ratios are 48% for $p + {}^{12}\mathrm{C}_{9.64}$ and 52% for $\alpha + {}^9\mathrm{B}_{g.s.}$.

A state at $E^* = 13.5$ MeV with $\Gamma \sim 500$ keV, $J^\pi = 3/2^+$ was observed in resonant proton scattering Ref. [44], somewhat wider than the structure observed here at 13.65 MeV. An even wider ($\Gamma \sim 6500$ keV) is reported by [45] but is probably unrelated to any structure in the present data. A

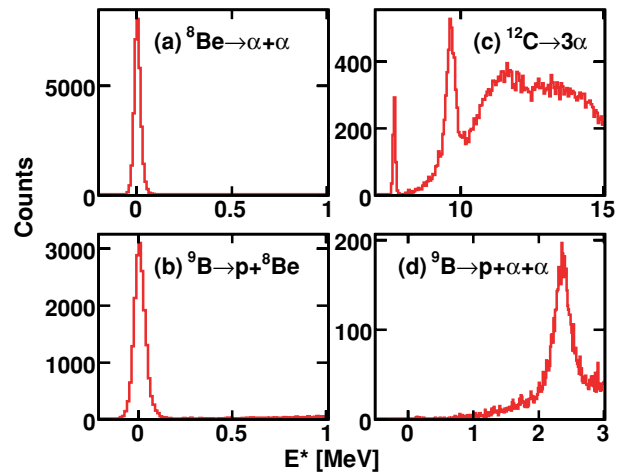

FIG. 22. (Color online) Excitation-energy distributions for the indicated subevents obtained from the $p + 3\alpha$ exit channel with both the C and Be targets.

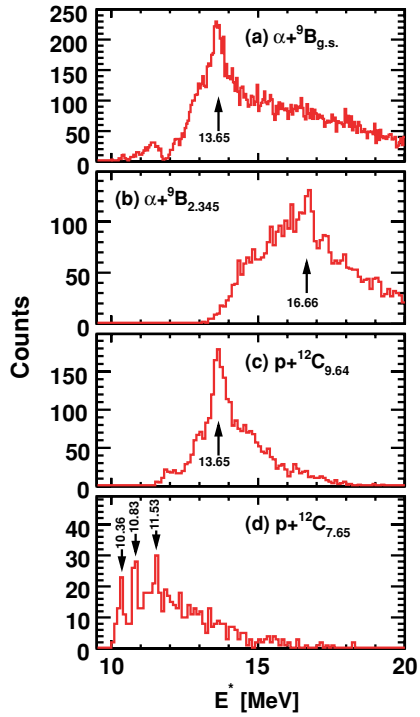

FIG. 23. (Color online) Excitation-energy distributions for ^{13}N nuclei determined for the indicated decay paths for both the C and Be targets. The arrows in (a)–(c) give the energies of previously unknown levels. In (d) the arrows show the location of known levels with energies consistent with the observed peaks.

previously unreported state at 16.66 MeV is observed in Fig. 23(b), associated with $\alpha + {}^{9}\mathrm{B}_{2.345}$ decay.

The spectrum for the $p + {}^{12}\mathrm{C}_{7.65}$ channel in Fig. 23(d) shows evidence of three peaks, which are labeled by the energies of three known ^{13}N levels [46]. Of the three peaks, the highest energy (11.53 MeV) state may be the most uncertain, as this peak is narrower than the experimental resolution of 300 keV. The widths of the other two peaks are consistent within the statistical error to the predicted resolution which is strongly energy dependent. The lowest energy peak at 10.36 MeV is consistent with a known doublet $(5/2^{-}, 7/2^{-})$. Both levels are very narrow: $\Gamma = 30$ and 60 keV, respectively. A state at $E^{*} = 10.83$ MeV has previously been assigned spin $1/2^{-}$ in the database.

From the $p + 3\alpha$ exit channel and the strong cluster nature of the intermediate states, one might expect the ^{13}N levels observed in this work to have a strong cluster structure. In the ^{13}C mirror nucleus, a number of rotational bands built on α-cluster configurations are predicted. These include positive and negative parity $K = 3/2$ bands associated with linear 3α chains, and oblate bands with the α particles arranged in an equilateral triangle [6].

The 10.36-MeV $5/2^{-}$ state is the analog of a 10.818-MeV state in ^{13}C which is purported to be the second member of a $K = 3/2^{-}$ band built on a linear α chain configuration [6]. Also, the analog of the 10.83-MeV state has been proposed as the bandhead of the $K = 3/2^{+}$ band in ^{13}C, although its $J^{\pi} = 1/2^{-}$ spin assignment in the database is inconsistent with this assignment. Possibly the ^{13}N state we observed is not the listed 10.83-MeV $J^{\pi} = 1/2^{-}$ level but a near degenerate $J = 3/2^{+}$ level or an $1/2^{+}$ state corresponding to an oblate configuration which is expected near this excitation energy [6]. The 13.65- and 16.66-MeV levels may be higher members of these rotational bands. The 13.65-MeV level is an excellent case for studying the angular correlations in order to deduce spin information, because, for both its decay branches, the intermediate states have nonzero spin. Unfortunately in the present work, the statistical errors due to the large background subtraction were too large to provide any information on the spin of this level.

Fujimura *et al.* [47] have made a detailed study of ^{13}N in a similar excitation-energy range using the (^{3}He,t) and (^{3}He,tp) reactions. However, apart from the 10.83-MeV state, the other states observed in the present work were not observed by Fujimura *et al*. This emphasizes the strong selectivity of the $3\alpha + p$ final state that presumably enhances these cluster states, which are not as easily excited by exchange reactions.

IV. CONCLUSIONS

Particle-unstable states in light nuclei have been investigated in $^{10}\mathrm{C} + \mathrm{Be}$, C collisions at $E/A = 10.7$ MeV. Excited states in ^{10}C were found that decay to the $2p + 2\alpha$ exit channels via a number of decay paths. These levels include a 5.22-MeV state that proton decays to the unstable ground state of ^{9}B, a 5.28-MeV state that undergoes the prompt three-body decay, $2p + {}^{8}\mathrm{Be}_{\mathrm{g.s.}}$, where the three-body correlations are intermediate between those reported for ${}^{6}\mathrm{Be}_{\mathrm{g.s.}}$ and ${}^{45}\mathrm{Fe}_{\mathrm{g.s.}}$ decays. Strength is found for three decay paths at $E^{*}(^{10}\mathrm{C}) \sim 6.5$ MeV. It is argued that there is a 6.55-MeV state with two branches, an 86% branch for sequential two-proton decay through the ${}^{9}\mathrm{B}_{\mathrm{g.s.}}$ intermediate state and a 14% branch for prompt two-proton decay. In the latter, the three-body correlations have a strong "diproton-like" character. In addition, a separate state at 6.56 MeV undergoes $\alpha + {}^{6}\mathrm{Be}_{\mathrm{g.s.}}$ decay. Finally, we observe a wide state at 8.4 MeV that proton decays to the 2.345-MeV level of ^{9}B. For the states with proton decay branches to the ground state of ^{9}B, angular correlations between the first two sequential decay axes indicate that these states have nonzero spin.

The three-body decay of the 2.345-MeV state of ^{9}B was examined, and the correlations were approximately described by a sequential decay scenario initiated by $\alpha + {}^{5}\mathrm{Li}_{\mathrm{g.s.}}$ decay. This result is at odds with a sequential decay through the broad first excited state of ^{8}Be reported for the mirror state in ^{9}Be [36].

Particle-unstable excited states are also seen in ^{10}B and ^{13}N nuclei. In ^{10}B, we have examined states observed by Leask *et al.* [43], and we confirm the existence of the 8.06- and 9.61-MeV states which decay via the $d + {}^{6}\mathrm{Li}_{2.186}$ channel. In ^{13}N, we observed a number of new states that decay into the $p + 3\alpha$ channel. Given the exit channel and the intermediate states (7.65- and 9.64-MeV excited states of ^{12}C and the ground state of ^{9}B) observed, these levels are expected to have a strong cluster structure.

ACKNOWLEDGMENTS

We would like to acknowledge useful discussions with F. C. Barker. This work was supported by the US Department of Energy, Division of Nuclear Physics, under Grant Nos. DE-FG02-87ER-40316, DE-FG02-93ER40773, and DE-FG02-04ER41320.

[1] D. Robson, Nucl. Phys. **A204**, 523 (1973).
[2] B. R. Fulton and W. D. M. Rae, J. Phys. G **16**, 333 (1990).
[3] R. J. Charity *et al.*, Phys. Rev. C **76**, 064313 (2007).
[4] R. J. Charity *et al.*, Phys. Rev. C **78**, 054307 (2008).
[5] M. Freer and A. C. Merchant, J. Phys. G **23**, 261 (1997).
[6] W. von Oertzen, M. Freer, and Y. Kanada-En'yo, Phys. Rep. **432**, 43 (2006).
[7] R. J. Charity, K. Mercurio, L. G. Sobotka, J. M. Elson, M. Famiano, A. Banu, C. Fu, L. Trache, and R. E. Tribble, Phys. Rev. C **75**, 051304 (2007).
[8] L. V. Grigorenko *et al.*, arXiv:0812.4065 (accepted for publication in Phys. Rev. C).
[9] L. V. Grigorenko, T. D. Wiser, K. Miernik, R. J. Charity, M. Pfutzner, A. Banu, C. R. Bingham, M. Cwiok, I. G. Darby, W. Dominik, J. M. Elson, T. Ginter, R. Grzywacz, Z. Janas, M. Karny, A. Korgul, S. N. Liddick, K. Mercurio, M. Rajabali, K. Rykaczewski, R. Shane, L. G. Sobotka, A. Stolz, L. Trache, R. E. Tribble, A. H. Wuosmaa, and M. V. Zhukov, Phys. Lett. **B677**, 30 (2009).
[10] K. Mercurio *et al.*, Phys. Rev. C **78**, 031602 (2008).
[11] R. E. Tribble, R. H. Burch, and C. A. Gagliardi, Nucl. Instrum. Methods A **285**, 441 (1989).
[12] M. S. Wallace *et al.*, Nucl. Instrum. Methods A **583**, 302 (2007).
[13] F. Ajzenberg-Selove, Nucl. Phys. **A523**, 1 (1991).
[14] D. R. Tilley, J. H. Kelly, J. L. Godwin, D. J. Millener, J. E. Purcell, C. G. Sheu, and H. R. Weller, Nucl. Phys. **A745**, 155 (2004).
[15] J. F. Ziegler, J. P. Biersack, and U. Littmark, *The Stopping and Range of Ions in Solids* (Pergamon, New York, 1985); the code SRIM can be found at www.srim.org.
[16] R. Anne, J. Herault, R. Bimbot, H. Gauvin, C. Bastin, and F. Hubert, Nucl. Instrum. Methods B **34**, 295 (1988).
[17] W. von Oertzen, Z. Phys. A **357**, 355 (1997).
[18] L. C. Biedenharn and M. E. Rose, Rev. Mod. Phys. **25**, 729 (1953).
[19] H. Frauenfelder, Annu. Rev. Nucl. Sci. **2**, 129 (1953).
[20] N. Mangelson, F. Ajzenberg-Selove, M. Reed, and C. C. Lu, Nucl. Phys. **88**, 137 (1966).
[21] L. Wang *et al.*, Phys. Rev. C **47**, 2123 (1993).
[22] A. S. Clough, C. J. Batty, B. E. Bonner, and L. E. Williams, Nucl. Phys. **A143**, 385 (1970).
[23] M. J. Schneider, B. W. Ridley, M. E. Rickey, J. J. Kraushaar, and W. R. Zimmerman, Phys. Rev. C **12**, 335 (1975).
[24] V. I. Goldansky, Nucl. Phys. **19**, 482 (1960).
[25] D. F. Geesaman, R. L. McGrath, P. M. S. Lesser, P. P. Urone, and B. VerWest, Phys. Rev. C **15**, 1835 (1977).
[26] Y. Kanada-En'yo and H. Horiouchi, Prog. Theor. Phys. Suppl. **142**, 205 (2001).
[27] J. Randrup, Comput. Phys. Commun. **59**, 439 (1990).
[28] R. A. Kryger *et al.*, Phys. Rev. Lett. **74**, 860 (1995).
[29] K. Miernik *et al.*, Phys. Rev. Lett. **99**, 192501 (2007).
[30] K. Miernik *et al.* (to be published in Eur. Phys. J. A).
[31] L. V. Grigorenko and M. V. Zhukov, Phys. Rev. C **68**, 054005 (2003).
[32] N. Curtis *et al.*, Phys. Rev. C **77**, 021301 (2008).
[33] H. T. Fortune and R. Sherr, Phys. Rev. C **73**, 064302 (2006).
[34] F. C. Barker, Phys. Rev. C **79**, 017302 (2009).
[35] E. Gete *et al.*, Phys. Rev. C **61**, 064310 (2000).
[36] P. Papka *et al.*, Phys. Rev. C **75**, 045803 (2007).
[37] S. E. Woosely, J. R. Wilson, G. J. Mathews, R. D. Hoffman, and B. S. Meyer, Astrophys. J. **433**, 229 (1994).
[38] K. Takahashi, J. Witti, and H. T. Janka, Astron. Astrophys. **286**, 857 (1994).
[39] A. M. Lane and R. G. Thomas, Rev. Mod. Phys. **30**, 257 (1958).
[40] E. K. Warburton, Phys. Rev. C **33**, 303 (1986).
[41] C. L. Woods, F. C. Barker, W. N. Catford, L. K. Fifield, and N. A. Orr, Aust. J. Phys. **41**, 525 (1988).
[42] F. C. Barker, Phys. Rev. C **68**, 054602 (2003).
[43] P. J. Leask *et al.*, Phys. Rev. C **63**, 034307 (2001).
[44] Y. Nagahara, J. Phys. Soc. Jpn. **16**, 133 (1961).
[45] D. F. Measday, M. Hasinoff, and D. L. Johnson, Can. J. Phys. **51**, 1227 (1973).
[46] F. Azjenberg-Selove, Nucl. Phys. **A523**, 1 (1991).
[47] H. Fujimura *et al.*, Phys. Rev. C **69**, 064327 (2004).